

Supersolid light in a semiconductor microcavity

J. L. Figueiredo,¹ J. T. Mendonça,¹ and H. Terças^{2,1}

¹*GoLP/Instituto de Plasmas e Fusão Nuclear, Instituto Superior Técnico, Universidade de Lisboa, 1049-001 Lisboa, Portugal*

²*Instituto Superior de Engenharia de Lisboa, Instituto Politécnico de Lisboa, Rua Conselheiro Emídio Navarro, 1959-0077 Lisboa, Portugal*

Supersolidity—simultaneous superfluid flow and crystalline order—has been realized in quantum atomic systems but remains unexplored in purely photonic platforms operating at weak light-matter coupling. We predict a supersolid phase of light in a plasma-filled optical microcavity, where photons acquire effective mass and interact via nonlocal, plasma-mediated nonlinearities. By deriving a Gross–Pitaevskii equation with a tunable photon-photon interaction kernel, we show that under coherent driving the cavity light field can spontaneously crystallize into a supersolid lattice via modulational instability. Crucially, this supersolid arises from a weak photon–electron coupling enabled by virtual electronic transitions, and it does not require hybrid polariton formation. Using doped semiconductor microcavities, we identify feasible conditions (electron densities $\sim 10^{10} - 10^{11} \text{ cm}^{-2}$ and optical intensities $\sim 10^2 - 10^4 \text{ W/cm}^2$) for experimental realization. This work establishes plasmonic cavities as a platform for correlated photonic matter with emergent quantum order.

PACS numbers:

Introduction— The realization of Bose–Einstein condensation (BEC) of photons in optical microcavities has opened a new frontier in quantum optics, with bosonic statistics and optical confinement combining to yield macroscopic coherence [1]. Pivotal experiments with dye-filled [2] and semiconductor [3] microcavities demonstrated that two-dimensional photon gases can thermalize and macroscopically occupy the cavity ground state when mirror curvature imparts an effective mass. These achievements established a close analogy with massive bosons and laid the foundation for subsequent explorations of quantum-fluid phenomena in light [4].

When effective photon–photon interactions are present, optical fields can display many-body behavior. In noncondensed optical media, related structures such as photonic solitons [5], vortex–antivortex pairs [6], and pattern formation [7, 8] are well established. By the same reasoning, analogous excitations should arise in condensed-light systems once interactions are properly engineered, leveraging macroscopic phase coherence to realize genuine quantum phases of light. The nature of photon interactions depends on the host medium, and while the atom-mediated case has been analyzed in depth [9–12], no comparable theory exists for the media in which photon BECs have been realized. In particular, photons in semiconductor microcavities couple predominantly to conduction- and valence-band electrons, hence understanding plasma-mediated photon–photon interactions is essential to exploit photon BECs as a pathway to quantum-fluid behavior of light.

In this Letter, we study the role of two-dimensional electron gases (2DEG) in mediating effective photon–photon interactions inside microcavities. We show how the electronic response leads to nonlocal photon–photon coupling, which can destabilize the homogeneous field and trigger the spontaneous emergence of supersolid

light. By integrating out the electronic degrees of freedom, we derive a driven–dissipative Gross–Pitaevskii (GP) equation for the intracavity field,

$$i\hbar \frac{\partial \mathbf{E}(\mathbf{r})}{\partial t} = \left[-\frac{\hbar^2}{2M} \nabla^2 + V_{\text{trap}}(\mathbf{r}) - i\hbar\kappa \right] \mathbf{E}(\mathbf{r}) + \hbar\Gamma \mathbf{E}_p(\mathbf{r}) + \int d\mathbf{r}' g(\mathbf{r} - \mathbf{r}') |\mathbf{E}(\mathbf{r}')|^2 \mathbf{E}(\mathbf{r}), \quad (1)$$

where M is the photon effective mass, κ and Γ the loss and pump rate, $\mathbf{E}_p(\mathbf{r})$ the pump field and $g(\mathbf{r})$ the plasma-induced interaction kernel, as we detail below. Unlike a local Kerr nonlinearity, $g(\mathbf{r})$ acquires an oscillatory, long-range form governed by the electronic response which shares key features with dipolar or spin-orbit coupled atomic BECs [13–15], hence establishing a new route to crystallization and supersolidity in weakly coupled photonic systems.

Photon field in a plasma environment— Consider an optical resonator with curved mirrors of radius R separated by a distance $d_0 \ll R$. Under ideal reflecting boundary conditions and sufficiently large lateral dimensions, the cavity supports a two-dimensional photon gas with an approximately quadratic dispersion relation for in-plane modes. In this paraxial regime, photons acquire an effective mass $M = \hbar\pi\ell/(\bar{c}^2 d_0)$, where \bar{c} is the light speed in the medium and ℓ is an integer arising from the transverse momentum quantization. In what follows, we focus on a single transverse mode of the cavity.

To generate an effective photon–photon interaction, we place a 2DEG inside the cavity. At the linear level, the plasma contributes with a refractive index shift $\sim \omega_p^2 \propto n_e$ [16, 17], with n_e denoting the electron density, but our interest is in the nonlinear regime where two photons can interact via the plasma [18]. Physically, a pair of photons can scatter by virtually exciting a plasma oscillation and exchanging momentum [19].

In the nonrelativistic regime, the total light-matter Hamiltonian is $\hat{H} = \hat{H}_e + \hat{H}_\gamma + \hat{H}_{\text{par.}} + \hat{H}_{\text{dia.}}$, where \hat{H}_e and \hat{H}_γ are the free electron and cavity-photon Hamiltonians, and $\hat{H}_{\text{par.}}$ and $\hat{H}_{\text{dia.}}$ describe the linear (*paramagnetic*) and nonlinear (*diamagnetic*) light-matter interactions, respectively [20]. Using the appropriate expansion basis, one finds:

$$\hat{H}_{\text{par.}} = \sum_{\mathbf{k}, \mathbf{k}', \mathbf{m}} \mathcal{M}_{\mathbf{k}, \mathbf{k}'}^{\mathbf{m}} (\hat{a}_{\mathbf{m}} + \hat{a}_{\mathbf{m}}^\dagger) \hat{c}_{\mathbf{k}+\mathbf{k}'}^\dagger \hat{c}_{\mathbf{k}'}, \quad (2)$$

$$\hat{H}_{\text{dia.}} = \sum_{\mathbf{k}, \mathbf{k}', \mathbf{n}, \mathbf{m}} \mathcal{I}_{\mathbf{k}, \mathbf{k}'}^{\mathbf{n}, \mathbf{m}} (\hat{a}_{\mathbf{n}} + \hat{a}_{\mathbf{n}}^\dagger) (\hat{a}_{\mathbf{m}} + \hat{a}_{\mathbf{m}}^\dagger) \hat{c}_{\mathbf{k}}^\dagger \hat{c}_{\mathbf{k}'}, \quad (3)$$

with $\mathcal{M}_{\mathbf{k}, \mathbf{k}'}^{\mathbf{m}} = \hbar e / (mV) \mathcal{A}_{\mathbf{m}}(\mathbf{k}) \cdot \mathbf{k}'$, $\mathcal{I}_{\mathbf{k}, \mathbf{k}'}^{\mathbf{n}, \mathbf{m}} = e^2 / (2mV) \int d\mathbf{r} e^{i\mathbf{r} \cdot (\mathbf{k}' - \mathbf{k})} \mathcal{A}_{\mathbf{n}}(\mathbf{r}) \cdot \mathcal{A}_{\mathbf{m}}(\mathbf{r})$, $\mathcal{A}_{\mathbf{m}}(\mathbf{k})$ denoting the Fourier transform of the vector-potential expansion coefficients $\mathcal{A}_{\mathbf{m}}(\mathbf{r})$, e the elementary charge and m the electron mass. As usual, $\hat{c}_{\mathbf{k}}^\dagger$ and $\hat{c}_{\mathbf{k}}$ denote the creation and annihilation electron operators, and $\hat{a}_{\mathbf{m}}^\dagger$ and $\hat{a}_{\mathbf{m}}$ their photonic counterpart.

Gross-Pitaevskii equation for cavity photons— To capture the effect of the plasma on the photon dynamics, we derive an effective Hamiltonian for the photon field by tracing out the electronic degrees of freedom. This is valid for regimes where the nominal photon energy largely exceeds $\hbar\omega_p$ and the plasma remains weakly perturbed. In the Supplemental Material [21], we show that eliminating the electron-photon interaction to order e^2 yields an effective photon field Hamiltonian of the form

$$\hat{H}' = \sum_{\mathbf{m}} \hbar\omega_{\mathbf{m}} \hat{a}_{\mathbf{m}}^\dagger \hat{a}_{\mathbf{m}} + \sum_{\mathbf{n}, \mathbf{m}, \mathbf{p}, \mathbf{q}} \gamma_{\mathbf{n}, \mathbf{m}}^{\mathbf{p}, \mathbf{q}} \hat{a}_{\mathbf{n}}^\dagger \hat{a}_{\mathbf{n}}^\dagger \hat{a}_{\mathbf{p}} \hat{a}_{\mathbf{q}}, \quad (4)$$

where

$$\gamma_{\mathbf{n}, \mathbf{m}}^{\mathbf{p}, \mathbf{q}} = -16 \sum_{\mathbf{k}, \mathbf{k}'} f_{\mathbf{k}'} (1 - f_{\mathbf{k}}) \frac{\mathcal{I}_{\mathbf{k}, \mathbf{k}'}^{\mathbf{q}, \mathbf{n}} (\mathcal{I}_{\mathbf{k}, \mathbf{k}'}^{\mathbf{p}, \mathbf{m}})^*}{\varepsilon_{\mathbf{k}} - \varepsilon_{\mathbf{k}'} + \hbar\omega_{\mathbf{n}} - \hbar\omega_{\mathbf{q}}}. \quad (5)$$

The summations above involve a product of electron distribution functions $f_{\mathbf{k}}$ stemming from the Fermi statistics, while the energy denominator contains the electron dispersion $\varepsilon_{\mathbf{k}} = \hbar^2 \mathbf{k}^2 / (2m)$.

In the limit of large photon-occupation numbers, $\langle \hat{a}_{\mathbf{n}}^\dagger \hat{a}_{\mathbf{n}} \rangle \gg 1$, the light field can be approximated by a coherent state, allowing a mean-field treatment. In this regime, the quantum operators are replaced by complex amplitudes and the dynamics of the electric field is governed by the nonlocal GP equation in Eq. (1) [21].

The most significant term of Eq. (1) is the interacting kernel $g(\mathbf{r})$ (see Eq. (23) of [21]), which determines the nature of photon-photon interactions from the electronic distribution. By moving to momentum space, the transformed kernel $g(\mathbf{k}) = \int d\mathbf{r} e^{-i\mathbf{k} \cdot \mathbf{r}} g(\mathbf{r})$ reads simply

$$g(\mathbf{k}) = \left(\frac{2e^4 \hbar}{m^2 \varepsilon_0 \omega_0^3} \right) \chi(\mathbf{k}, \omega = 0), \quad (6)$$

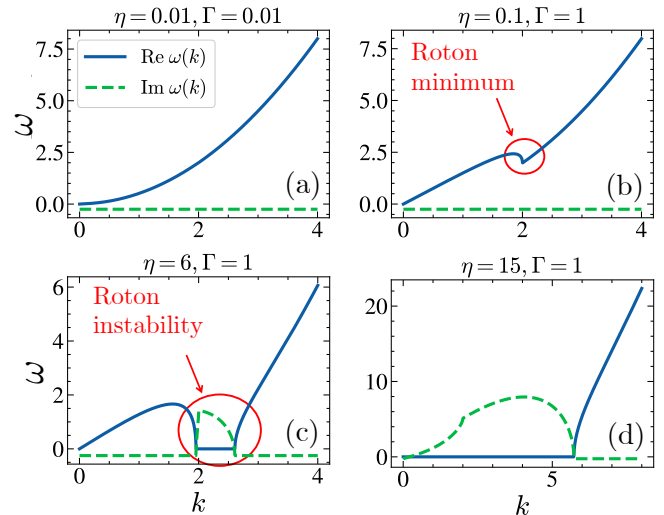


FIG. 1: Excitation spectrum in Eq. (9) as function of the local coupling η and pump rate Γ . Increasing the attractive contact interaction, or equivalently the pump rate, drives the spectrum from quadratic (noninteracting limit) to a roton-like form with a finite- k minimum. Instability sets in when the roton gap closes, driven by increasing photon-photon interactions. In all cases, we have fixed the nonlocal coupling and the loss rate to $\alpha = 1$ and $\kappa = 0.25$, respectively. All relevant physical quantities are normalized as in Ref. [22]

where $\chi(\mathbf{k}, \omega)$ is the Lindhard response function,

$$\chi(\mathbf{k}, \omega) = \frac{1}{V} \sum_{\mathbf{k}'} \frac{f_{\mathbf{k}' - \mathbf{k}} - f_{\mathbf{k}'}}{\varepsilon_{\mathbf{k}' - \mathbf{k}} - \varepsilon_{\mathbf{k}'} + \hbar\omega + i\delta^+}. \quad (7)$$

that measures the polarizability of a Fermi gas. Here, the latter quantifies the effective photon-photon interaction, as it represents how the electronic polarization induced by one photon influences the interaction with a second. For nondegenerate electron bands, the distribution function is of Boltzmann type, $f_{\mathbf{k}} \equiv f(\varepsilon_{\mathbf{k}}) = 4\pi n \lambda_B^2 e^{-\varepsilon_{\mathbf{k}} / k_B T_e}$ with $\lambda_B = \hbar / \sqrt{2mk_B T_e}$ being the de Broglie length and T_e the electron temperature. In this case, we get $g(\mathbf{r}) = -\eta \delta(\mathbf{r})$ with $\eta = 2e^4 \hbar n / (m^2 \varepsilon_0 \omega_0^3 k_B T_e)$, thereby resulting in a *purely attractive* Kerr interaction. In contrast, for a highly-degenerate plasma in the $T \rightarrow 0$ limit, $f_{\mathbf{k}} = 2\Theta(k_F - k)$, with $k_F = (2\pi n)^{1/2}$ the Fermi wavevector and $\Theta(x)$ the Heaviside-step function. This leads to a nonlocal interaction of the form $g(r) = \alpha G(k_F r)$, with

$$G(r) = \frac{\sin(2r) - 2r \cos(2r)}{r^3}, \quad (8)$$

and $\alpha = 4e^4 k_F^4 / (\pi^4 \hbar m \varepsilon_0 \omega_0^3)$. The nonlocal and oscillatory behavior implies that the photon-photon interaction is not simply a contact nonlinearity as in a conventional Kerr medium. Instead, it features spatially extended regions where the effective interaction alternates in sign (attractive vs. repulsive), bearing similarities with dipolar interactions in atomic BECs responsible for the formation of supersolid matter states [23].

Roton instability and supersolidity— The dynamical analogy between cavity photons and dipolar BECs raises a natural question of whether the cavity field can undergo an analogous evolution to a supersolid phase. To address this question, we examine the dispersion of collective excitations obtained from the linearized GP equation (1),

$$\hbar\omega(k) = \sqrt{\varepsilon_k [\varepsilon_k + 2N_0g(k)]} - i\hbar\kappa, \quad (9)$$

where $N_0 = |\mathbf{E}_0|^2$. The later is fixed by the zero-*th* order equation according to $N_0 = \Gamma^2 |\mathbf{E}_p|^2 / (\kappa^2 + [N_0g_0/\hbar]^2)$, where we defined $g_0 \equiv g(\mathbf{k} = 0) = \int d\mathbf{r} g(\mathbf{r})$.

The emergence of a *supersolid* requires two conditions to hold simultaneously [24–26]. i) The long-wavelength mode must remain *superfluid*, which means the dispersion must verify $\omega \sim v_s k$ as $k \rightarrow 0$. Since $v_s^2 = N_0 g(0)$ we require $g(0) > 0$, otherwise the $k \rightarrow 0$ mode is unstable. ii) A finite- k band must soften and become unstable. From Eq. (9), exponential growth occurs when $\varepsilon_k [\varepsilon_k + 2N_0g(k)] < -\kappa^2$. In the high-reflectivity limit $\kappa \rightarrow 0$ this reduces to the roton-gap closure condition $\varepsilon_{k_*} + 2N_0g(k_*) = 0$ at some roton wavenumber $k_* \neq 0$. Practically, this means $g(k)$ must be positive near $k = 0$ but negative in a finite region around k_* so the density modulations at wavelength $2\pi/k_*$ grow while high- k modes remain stabilized by ε_k .

In regimes where the photon field perturbs the medium only weakly – or on timescales short compared to the 2DEG relaxation time – the distribution function $f_{\mathbf{k}}$ can be treated as stationary (e.g., in thermal equilibrium). Consequently, $g(\mathbf{k})$ reduces to the corresponding static response function. For both the degenerate ($T \ll T_F$, with T_F denoting the Fermi temperature) and thermal ($T \gg T_F$) limits of the Fermi-Dirac function, the integral in Eq. (7) can be performed, and we are led to

$$g(k) = \begin{cases} -\eta & T \gg T_F, \\ 2\pi\alpha \sqrt{4 - \frac{k^2}{k_F^2}} \Theta\left(2 - \frac{k}{k_F}\right) & T \ll T_F. \end{cases} \quad (10)$$

Individually, both degenerate and nondegenerate 2DEGs yield a sign-definite $g(\mathbf{k})$, which precludes supersolidity. To induce and control the required sign change, we employ two electronically isolated semiconductor quantum wells (QW) in the following scheme: a first QW (say, QW1) hosts a degenerate 2DEG with Fermi level E_F (resp. Fermi wavevector k_F), while QW2 hosts a nondegenerate one. A wide-gap barrier suppresses tunneling and Coulomb drag, ensuring that the distributions remain independent and stationary. The cavity mode couples to each sheet with controllable weights w_j , yielding an effective kernel for Eq. (1) of the form

$$g(k) = w_1 g_{\text{deg}}(k) + w_2 g_{\text{th}}(k), \quad (11)$$

with g_{deg} and g_{th} given in Eq. (10), and constants w_j controlled by the position of QW j along the optical path

of the transverse field ($w_1 = w_2 = 1$ for symmetrically disposed QWs).

In Fig. 1, we depict the excitation spectrum (9) computed with the effective interaction in Eq. (11) for four representative regimes [22]. When both the local coupling (η) and pumping strength (Γ) are weak, the spectrum is fully stable and parabolic, $\omega \sim k^2$, so photons propagate essentially ballistically. For moderate values of η , the dispersion acoustic at the origin, $\omega \sim k$, and a roton minimum at finite k_* , signaling enhanced correlations and compatibility with superfluid response [27–29]. Interestingly, unlike usual rotons in dipolar BECs, the minimum group velocity diverges due to the cusp developed in ω at k_* . This is a consequence of the Kohn anomaly patent in the Fourier components of the interaction [30–32], as shown in Eq. (10). Pushing the parameters further, $\text{Re } \omega$ crosses zero over a finite interval around k_* , while $\text{Im } \omega(k_*) > 0$ marks the onset of a modulational instability.

Dynamics of supersolid formation— To corroborate the analytical stability analysis, we performed numerical simulations of the driven-dissipative GP equation (1) on a spatial grid using a split-step Fourier method and periodic boundary conditions. A fast Fourier transform algorithm was used to compute the nonlocal contribution via the convolution theorem. The normalized cavity field is initialized to a complex white-noise distribution to mimic vacuum fluctuations in the initially empty cavity [22].

In summary, the field either remains homogeneous or develops spatial modulations in $|E|^2$, and a clear threshold behavior in the pump intensity is observed. For subcritical Γ , the uniform solution $E \simeq -i\Gamma E_p/\kappa$ persists, damping any small perturbation while the phase locks to the pump laser. Above a critical drive, the uniform state becomes unstable and small fluctuations grow exponentially, akin to optically-driven atomic BECs [33]. In regimes where the nonlocal term dominates over the local nonlinearity, the system favors periodically modulated solutions due to the effective negative pressure at a finite length scale. For $\eta \gtrsim \alpha$, the evolution tends toward collapse into unsteady filaments rather than an periodic pattern. Hence, a supersolid emerge when these competing interactions balance (see Ref. [34] for a comparison with dipolar BECs).

When the nonlocal interaction is weak ($\alpha < 1$), or the local nonlinearity vs. dissipation balance favors a uniform state, the system remains in a homogeneous *superfluid* phase. In this regime [Fig. 1(b)], $E(\mathbf{r}, t)$ approaches a steady, nearly uniform state across the domain. The structure factor $S(k)$ has a single peak at $k = 0$, indicating no crystalline density modulation. Meanwhile, the phase remains coherent throughout the system with a large fraction of excitations in the $k = 0$ mode, corresponding to a superfluid fraction close to unit (see the video with a representative time evolution of the superfluid phase in Supplemental Material [21]).

If interactions are increased until an instability is

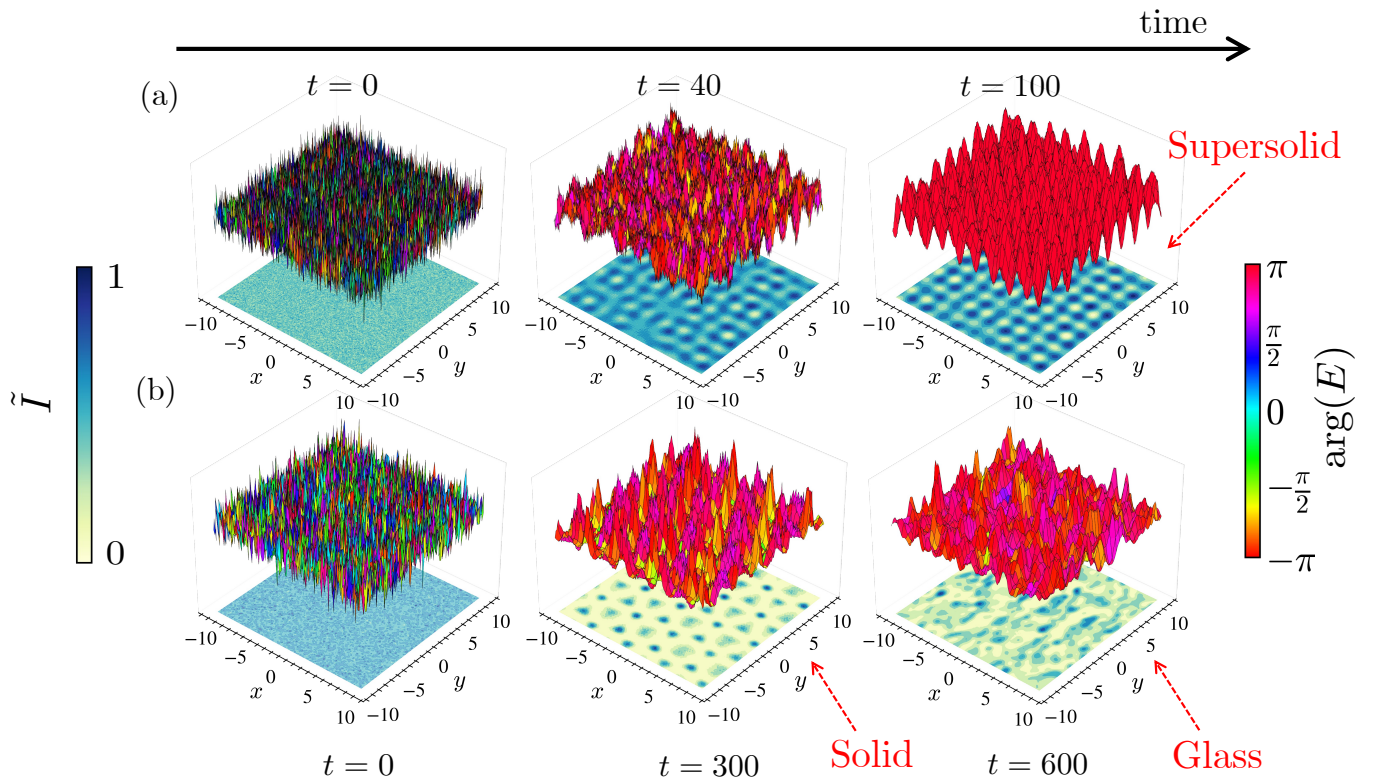


FIG. 2: Time evolution of the intracavity normalized field amplitude $\tilde{I}(t) = (|E(t)|^2 - \min |E(t)|^2) / (\max |E(t)|^2)$ and phase indicated by the color of the curve at each point. (a) For parameters favoring nonlocal interactions, a periodic density modulation forms while global phase coherence is attained, yielding a supersolid in steady-state. (b) For stronger local interactions, the system evolves into a solid without coherence (middle panel) and eventually a disordered glassy state (right panel). Parameters used are the same as those of Fig. 1(c)–(d), respectively. Animations of these simulations are given in Supplemental Material [21]. All relevant physical quantities are normalized as in Ref. [22].

reached [see Fig. 1(c)], the system can sustain exponential growth of k -modes localized around $k_* \simeq 2k_F$ while steady-state phase coherence is induced by nonlocal photon-photon interactions, *i.e.*, the phase becomes essentially uniform across the entire domain. This implies that the system still behaves as a single macroscopic wavefunction, even though the density is non-uniform, signaling the formation of a *supersolid*. The time evolution of supersolid formation is depicted in Fig. 2(a), where both the amplitude and the phase of $E(\mathbf{r}, t)$ converge toward a periodic array of density peaks embedded in a background condensate with uniform phase.

Continuing to increase the local interaction while keeping the nonlocal interaction strength fixed favors amplitude instability while spoiling phase coherence. When global phase coherence is lost, the result is not a true supersolid but rather a transient crystal without superfluid properties, as represented in Fig. 2(b). At intermediate time $t = 300M/(\hbar k_F^2)$, a solid is formed as a result of maximum instability for a given mode k_* , which is progressively destroyed due to a broad range of k modes verifying $\text{Im}\omega(k) > 0$. At later times, a fluctuating glassy cloud with some local clustering but no long-range order

emerges.

The phase diagrams in Fig. (1) summarize the outcomes of our steady-state GP simulations across the control knobs. The arrows labeled “crystallization” and “phase ordering” emphasize the separation of dynamical time scales seen above in the fast selection of k_* from the unstable band set by $[\text{Im}\omega(k_*)]^{-1}$, followed by slower phase alignment. For the cuts shown, the unstable band is centered at $k_* \simeq 1.5\text{--}2 k_F$, implying a lattice spacing $a \sim 2\pi/k_* \simeq 3\text{--}4 k_F^{-1}$. Increasing the nonlocal coupling α widens the supersolid wedge and shifts k_* to larger values, while increasing the local attraction η narrows the wedge and ultimately drives a transition to an incoherent solid/glass, consistent with Fig. 1.

Experimental setup— In order to experimentally achieve the supersolid phase controlled by Eq. (11), we propose a planar GaAs/AlAs diffracted Bragg mirror (DBR) microcavity with a GaAs spacer containing two n -type GaAs QWs and operating at room temperature. Each QW is positioned at consecutive longitudinal antinodes and separated by $\text{Al}_{0.9}\text{Ga}_{0.1}$ layer $\sim 30\text{--}50$ nm to suppress tunneling and interlayer drag. Using modulation doping and transparent gates, QW1 is tuned *degen-*

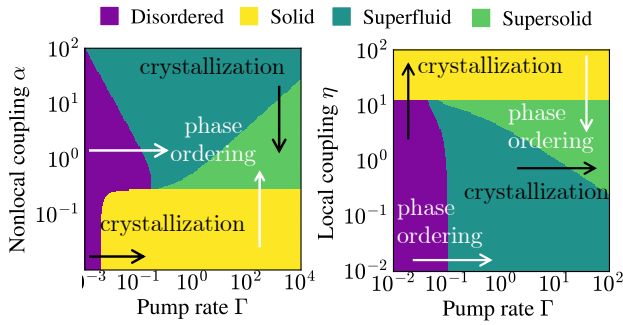


FIG. 3: Phase diagrams of the driven-dissipative GP model showing steady states as a function of pump rate Γ and (right) nonlocal coupling α or (left) local coupling η . Regions correspond to disordered, superfluid, solid, and supersolid phases. Arrows indicate the separation of dynamical time scales: fast crystallization at finite k followed by slower phase ordering. Fixed parameters are $\kappa = 0.1$, $\eta = 1$ or $\alpha = 1$ [22].

erate with sheet density $n_1 \simeq (4-10) \times 10^{11} \text{ cm}^{-2}$, yielding a Fermi temperature $T_F \simeq 160-450 \text{ K}$, while QW2 is *nondegenerate* with $n_2 \simeq (1-3) \times 10^{10} \text{ cm}^{-2}$, giving $T_F \simeq 4-12 \text{ K}$. A near-resonant, sub-gap continuous-wave (CW) pump laser at 950 nm addresses the $k \simeq 0$ cavity mode with detuning $\Delta = \pm(1-3) \text{ meV}$, 20–30 μm spot, and on-sample power 0.1–1 mW, keeping hole creation negligible. Placing the QWs at antinodes yields controllable photonic weights w_1 and w_2 in the mixed kernel $g(k) = w_1 g_{\text{deg}}(k) + w_2 g_{\text{th}}(k)$, enabling a finite- k sign change compatible with supersolidity (for additional design and operation details, see [21]).

For typical semiconductor-microcavity dimensions, we expect a photon mass of order $M \sim 10^{-5} m_e$, which places the interaction parameter in the range $\eta \sim (10^{-5}-10^{-3}) \times [I_p / (1 \text{ W m}^{-2})]$ across realistic densities and temperatures, with I_p the pump intensity. Likewise, $\alpha \sim 1.4 \times 10^{-4} \times [I_p / (1 \text{ W m}^{-2})]$, where the prefactor depends only on M . These scalings show that the conditions required to access the supersolid regime are well within reach using low to moderate pump intensities.

Conclusions— In summary, we have shown that a weakly-coupled optical microcavity containing 2D electron gases can support a supersolid phase of light as predicted by the generalized GP equation. Above a critical threshold, the system spontaneously forms a periodic lattice of light while retaining global phase coherence, thereby realizing a supersolid state. Notably, this supersolid arises in a purely photonic regime without relying on excitonic polariton formation, distinguishing it from previously observed polariton supersolids [35, 36]. We derived a Gross-Pitaevskii-type equation governing the cavity photon gas and provided analytical and numerical evidence for the supersolid transition. Importantly, our calculations identify experimentally accessible conditions for observing supersolid light. We find that electron densities of $\sim 10^{10} - 10^{11} \text{ cm}^{-2}$ and optical intensities of $\sim 10^2 - 10^4 \text{ W/cm}^2$ are sufficient in a high- Q semiconductor microcavity. Such parameters are well within the range of modern semiconductor cavity experiments, indicating that the creation of a supersolid light lattice is feasible with current technology.

Our work provides the first evidence for a purely-photonic supersolid, paving the way for exploring strongly correlated phases of light in driven-dissipative systems by identifying how to manipulate the effective photon-photon coupling through plasma parameters. Moreover, a photonic supersolid, as proposed here, could serve as a novel platform for quantum simulation of many-body physics and might inspire new photonic devices that harness the unique combination of coherence and rigidity in a light crystal.

Acknowledgments— J. L. F. acknowledges Fundação para a Ciência e a Tecnologia (FCT-Portugal) through the Grant No. UI/BD/151557/2021.

Data availability— The data that support the findings of this Letter are not publicly available upon publication because it is not technically feasible and/or the cost of preparing, depositing, and hosting the data would be prohibitive within the terms of this research project. The data are available from the authors upon reasonable request

-
- [1] A. Kruchkov, *Phys. Rev. A* **89**, 033862 (2014).
 - [2] J. Klaers, F. Vewinger, and M. Weitz, *Nature Physics* **6**, 512 (2010).
 - [3] R. C. Schofield, M. Fu, E. Clarke, I. Farrer, A. Trapalis, H. S. Dhar, R. Mukherjee, T. Severs Millard, J. Heffernan, F. Mintert, R. A. Nyman, and R. F. Oulton, *Nature Photonics* **18**, 1083 (2024).
 - [4] I. Carusotto and C. Ciuti, *Reviews of Modern Physics* **85**, 299 (2013).
 - [5] J. W. Fleischer, M. Segev, N. K. Efremidis, and D. N. Christodoulides, *Nature* **422**, 147 (2003).
 - [6] C. Wan, Q. Cao, J. Chen, A. Chong, and Q. Zhan, *Nature Photonics* **16**, 519 (2022).
 - [7] C. Whittaker, B. Dzurnak, O. Egorov, G. Buonaiuto, P. Walker, E. Cancellieri, D. Whittaker, E. Clarke, S. Gavrillov, M. Skolnick, *et al.*, *Physical Review X* **7**, 031033 (2017).
 - [8] E. I. Kiselev and Y. Pan, *Physical Review A* **111**, 053509 (2025).
 - [9] R. Y. Chiao, T. H. Hansson, J. M. Leinaas, and S. Viefers, *Phys. Rev. A* **69**, 063816 (2004).
 - [10] Y. Yang, J. Lu, and L. ZHou, *Optics Express* **31**, 39784 (2023).
 - [11] M. Heuck, K. Jacobs, and D. R. Englund, *Physical Review A* **101**, 042322 (2020).
 - [12] A. V. Gorshkov, J. Otterbach, M. Fleischhauer, T. Pohl,

- and M. D. Lukin, *Phys. Rev. Lett.* **107**, 133602 (2011).
- [13] B. B. e. a. Baizakov, *Phys. Rev. A* **84**, 033621 (2011).
- [14] M. A. Khamehchi, Y. Zhang, C. Hamner, T. Busch, and P. Engels, *Phys. Rev. A* **90**, 063624 (2014).
- [15] J. Léonard, A. Morales, P. Zupancic, T. Esslinger, and T. Donner, *Nature* **543**, 87–90 (2017).
- [16] J. D. Jackson, *Classical Electrodynamics*, 3rd ed. (John Wiley & Sons, Nashville, TN, 1998).
- [17] J. Mendonça and H. Terças, *Physical Review A* **95**, 063611 (2017).
- [18] J. Figueiredo, J. Mendonça, and H. Terças, *Physical Review E* **108**, L013201 (2023).
- [19] J. L. Figueiredo, J. T. Mendonça, and H. Terças, *Phys. Rev. A* **110**, 063519 (2024).
- [20] C. Cohen-Tannoudji, J. Dupont-Roc, and G. Grynberg, *Atom-photon interactions: basic processes and applications* (John Wiley & Sons, 2024).
- [21] Check the Supplemental Material located at [URL] for details on the derivation of the plasma mediated photon-photon interaction.
- [22] For numerical purposes, we adimensionalize all physical quantities. Time variables are given in units of $M/\hbar k_F^2$, distances in $1/k_F$, and electric fields in $|\mathbf{E}_p|$. Moreover, the local coupling η , with dimension of energy/(electric field)², is normalized to $\hbar^2 k_F^2/(2M|\mathbf{E}_p|^2)$, while its nonlocal counterpart α , with dimensions of energy/(distance \times electric field²), is given in units of $\hbar^2 k_F^4/(M|\mathbf{E}_p|^2)$.
- [23] A. Alaña, I. n. L. Egusquiza, and M. Modugno, *Phys. Rev. A* **108**, 033316 (2023).
- [24] H. Deng, H. Haug, and Y. Yamamoto, *Rev. Mod. Phys.* **82**, 1489 (2010).
- [25] E. Poli, D. Baillie, F. Ferlaino, and P. B. Blakie, *Phys. Rev. A* **110**, 053301 (2024).
- [26] M. Boninsegni and N. V. Prokof'ev, *Rev. Mod. Phys.* **84**, 759 (2012).
- [27] N. Bogoliubov, *J. Phys* **11**, 23 (1947).
- [28] A. J. Leggett, *Rev. Mod. Phys.* **71**, S318 (1999).
- [29] P. Hohenberg and P. Martin, *Annals of Physics* **34**, 291 (1965).
- [30] S. H. Koenig, *Phys. Rev.* **135**, A1693 (1964).
- [31] S. Piscanec, M. Lazzeri, F. Mauri, A. C. Ferrari, and J. Robertson, *Phys. Rev. Lett.* **93**, 185503 (2004).
- [32] R. M. Martin, *Electronic structure* (Cambridge University Press, Cambridge, England, 2004).
- [33] Y.-C. Zhang, V. Walther, and T. Pohl, *Phys. Rev. Lett.* **121**, 073604 (2018).
- [34] A. Maluckov, G. Gligorić, L. c. v. Hadžievski, B. A. Malomed, and T. Pfau, *Phys. Rev. Lett.* **108**, 140402 (2012).
- [35] D. Trypogeorgos, A. Gianfrate, M. Landini, D. Nigro, D. Gerace, I. Carusotto, F. Riminucci, K. W. Baldwin, L. N. Pfeiffer, G. I. Martone, M. De Giorgi, D. Ballarini, and D. Sanvitto, “Emerging supersolidity from a polariton condensate in a photonic crystal waveguide,” (2024).
- [36] X. Zhai, C. Xing, X. Yang, X. Zhang, H. Dai, X. Wang, A. Pan, S. Schumacher, X. Ma, and T. Gao, “Electrically tunable nonrigid moire exciton polariton supersolids at room temperature,” (2025).

Supplemental Material: Supersolid light in a semiconductor microcavity

I. PHOTON-PHOTON INTERACTIONS IN THE PRESENCE OF BACKGROUND PLASMA

The interaction between cavity photons and plasma electrons leads to significant modifications of the photon dynamics. To capture these effects, one can derive an effective Hamiltonian for the photon field by integrating out the electronic degrees of freedom. In the regime where the photon energy is far from electronic resonances and the plasma remains weakly perturbed, the role of the plasma is to mediate an effective photon-photon interaction. This interaction emerges from virtual electronic transitions induced by the nonlinear light-matter potential, akin to the role of virtual phonons in mediating attractive electron-electron interactions arising in low-temperature superconductors.

Using the rotating-wave approximation (RWA), the total electron-photon Hamiltonian can be reduced to $\hat{H} = \hat{H}_0 + \hat{V}$, where \hat{H}_0 denotes the plasma and photon kinetic terms and

$$\hat{V} = \sum_{\mathbf{k}, \mathbf{k}', \mathbf{n}, \mathbf{m}} \mathcal{I}_{\mathbf{k}, \mathbf{k}'}^{\mathbf{n}, \mathbf{m}} (\hat{a}_{\mathbf{n}} \hat{a}_{\mathbf{m}}^\dagger + \hat{a}_{\mathbf{n}}^\dagger \hat{a}_{\mathbf{m}}) \hat{c}_{\mathbf{k}}^\dagger \hat{c}_{\mathbf{k}'} \quad (1)$$

is the number-conserving and resonant part of the light-matter interaction.

From perturbation theory, it is possible to eliminate light-matter interactions to leading order by performing an unitary transformation as described in Ref. [1]. The rotated Hamiltonian $\hat{H}' = \hat{U} \hat{H} \hat{U}^\dagger$ then contains purely photon-photon interactions of the form

$$\hat{H}' = \sum_{\mathbf{m}} \hbar \omega_{\mathbf{m}} \hat{a}_{\mathbf{m}}^\dagger \hat{a}_{\mathbf{m}} + \sum_{\mathbf{n}, \mathbf{m}, \mathbf{p}, \mathbf{q}} \gamma_{\mathbf{n}, \mathbf{m}}^{\mathbf{p}, \mathbf{q}} \hat{a}_{\mathbf{n}}^\dagger \hat{a}_{\mathbf{m}}^\dagger \hat{a}_{\mathbf{p}} \hat{a}_{\mathbf{q}} + \dots, \quad (2)$$

with $\gamma_{\mathbf{n}, \mathbf{m}}^{\mathbf{p}, \mathbf{q}}$ denoting the amplitude for events involving four photons and \dots standing for the remaining higher-order terms. Three-photon processes are absent under the RWA since these involve mixing of modes that cannot simultaneously conserve energy and momentum in a uniform medium. To determine the form of $\gamma_{\mathbf{n}, \mathbf{m}}^{\mathbf{p}, \mathbf{q}}$, let $|i\rangle$ be a state with two photons in modes \mathbf{p} and \mathbf{q} , $|i\rangle = \hat{a}_{\mathbf{p}}^\dagger \hat{a}_{\mathbf{q}}^\dagger |\Phi\rangle$, and $|\Phi\rangle$ an arbitrary plasma state. Similarly, $|f\rangle = \hat{a}_{\mathbf{n}}^\dagger \hat{a}_{\mathbf{m}}^\dagger |\Phi\rangle$ denotes a final state with two photons in modes \mathbf{n} and \mathbf{m} . The first term in the perturbation expansion reads

$$\gamma_{\mathbf{n}, \mathbf{m}}^{\mathbf{p}, \mathbf{q}} = - \sum_{j \in \text{process}} \frac{\langle f | \hat{V} | j \rangle \langle j | \hat{V} | i \rangle}{E_j - E_i}, \quad (3)$$

with E_j and E_i the kinetic energy of states $|j\rangle$ and $|i\rangle$.

There are essentially four channels for which the numerator in Eq. (3) is nonzero. Since the action of \hat{V} on a many-body state returns a new state with the same number of total excitations, then this corresponds to moving

one photonic and one fermionic excitations from a given state to another. This means that the intermediate state $|j\rangle$ must differ from $|i\rangle$ by having either:

- (1) the photon in mode \mathbf{q} moved to mode \mathbf{n} ,
- (2) the photon in mode \mathbf{q} moved to mode \mathbf{m} ,
- (3) the photon in mode \mathbf{p} moved to mode \mathbf{n} ,
- (4) the photon in mode \mathbf{p} moved to mode \mathbf{m} .

These correspond to the four different Feynman diagrams for the process, each with a different energy denominator. As an example, let us consider the case (1), where the action of $\hat{a}_{\mathbf{n}}^\dagger \hat{a}_{\mathbf{q}}$ is followed by $\hat{a}_{\mathbf{m}}^\dagger \hat{a}_{\mathbf{n}}$. For this process, the denominator reads

$$\frac{1}{E_j - E_i} = \frac{1}{\varepsilon_{\mathbf{k}} - \varepsilon_{\mathbf{k}'} + \hbar \omega_{\mathbf{n}} - \hbar \omega_{\mathbf{q}}}, \quad (4)$$

while the numerator is

$$\begin{aligned} \langle f | \hat{V} | j \rangle \langle j | \hat{V} | i \rangle &= \sum_{\mathbf{k}, \mathbf{k}'} \sum_{\mathbf{k}'', \mathbf{k}'''} \mathcal{I}_{\mathbf{k}, \mathbf{k}'}^{\mathbf{q}, \mathbf{n}} \left(\mathcal{I}_{\mathbf{k}'', \mathbf{k}'''}^{\mathbf{p}, \mathbf{m}} \right)^* \langle \Phi | \hat{c}_{\mathbf{k}''}^\dagger \hat{c}_{\mathbf{k}'''} \hat{c}_{\mathbf{k}}^\dagger \hat{c}_{\mathbf{k}'} | \Phi \rangle. \end{aligned} \quad (5)$$

Using the anti-commutation relations of plasma operators, one can show that

$$\langle \Phi | \hat{c}_{\mathbf{k}''}^\dagger \hat{c}_{\mathbf{k}'''} \hat{c}_{\mathbf{k}}^\dagger \hat{c}_{\mathbf{k}'} | \Phi \rangle = \delta_{\mathbf{k}', \mathbf{k}''} \delta_{\mathbf{k}, \mathbf{k}'''} f_{\mathbf{k}'} (1 - f_{\mathbf{k}}), \quad (6)$$

where $f_{\mathbf{k}} = \langle \Phi | \hat{c}_{\mathbf{k}}^\dagger \hat{c}_{\mathbf{k}} | \Phi \rangle$ is the plasma distribution function. The contribution from this process becomes

$$\gamma_{\mathbf{n}, \mathbf{m}}^{\mathbf{p}, \mathbf{q}} \Big|_{\text{process 1}} = -4 \sum_{\mathbf{k}, \mathbf{k}'} \frac{\mathcal{I}_{\mathbf{k}, \mathbf{k}'}^{\mathbf{q}, \mathbf{n}} \left(\mathcal{I}_{\mathbf{k}, \mathbf{k}'}^{\mathbf{p}, \mathbf{m}} \right)^* f_{\mathbf{k}'} (1 - f_{\mathbf{k}})}{\varepsilon_{\mathbf{k}} - \varepsilon_{\mathbf{k}'} + \hbar \omega_{\mathbf{n}} - \hbar \omega_{\mathbf{q}}}, \quad (7)$$

where the factor of 4 accounts for the degeneracy. The other three cases can be easily found by following the same procedure. When all four contributions are found, one can exploit the symmetries of these amplitudes and arrive at Eq. (5) of the main text,

$$\gamma_{\mathbf{n}, \mathbf{m}}^{\mathbf{p}, \mathbf{q}} = -16 \sum_{\mathbf{k}, \mathbf{k}'} f_{\mathbf{k}'} (1 - f_{\mathbf{k}}) \frac{\mathcal{I}_{\mathbf{k}, \mathbf{k}'}^{\mathbf{q}, \mathbf{n}} \left(\mathcal{I}_{\mathbf{k}, \mathbf{k}'}^{\mathbf{p}, \mathbf{m}} \right)^*}{\varepsilon_{\mathbf{k}} - \varepsilon_{\mathbf{k}'} + \hbar \omega_{\mathbf{n}} - \hbar \omega_{\mathbf{q}}}. \quad (8)$$

II. DERIVATION OF THE GROSS-PITAIEVSKII EQUATION

In this section we derive the effective Gross-Pitaevskii (GP) equation governing the evolution of the complex electric field $\mathbf{E}^{(+)}(\mathbf{r}, t)$ under the photon-photon interaction term of Eq. (2).

Let $\phi_{\mathbf{n}}(t) \equiv \langle \hat{a}_{\mathbf{n}} \rangle$ denote the expectation value of photon annihilation operators. Equivalently, we may write

$\hat{a}_{\mathbf{n}} = \phi_{\mathbf{n}} + \delta\hat{a}_{\mathbf{n}}$, where $\delta\hat{a}_{\mathbf{n}}$ is the quantum fluctuation verifying $\langle \delta\hat{a}_{\mathbf{n}} \rangle = 0$. The classical electric field of the photon gas $\mathbf{E}(\mathbf{r}, t)$ is fully determined by the set $\{\phi_{\mathbf{n}}\}$ due to its linear expansion in photon operators. Since the GP equation in general determines a complex solution, it is convenient to separate $\mathbf{E}(\mathbf{r}, t)$ in the positive and negative frequency components, $\mathbf{E}(\mathbf{r}, t) = \mathbf{E}^{(+)}(\mathbf{r}, t) + \mathbf{E}^{(-)}(\mathbf{r}, t)$, where

$$\mathbf{E}^{(+)}(\mathbf{r}, t) = \sum_{\mathbf{m}} \mathcal{E}_{\mathbf{m}}(\mathbf{r}) \phi_{\mathbf{m}}(t) \quad (9)$$

and $\mathbf{E}^{(-)} = [\mathbf{E}^{(+)}]^*$. The electric-field coefficients are related with $\mathcal{A}_{\mathbf{m}}(\mathbf{r})$ through the relation $\mathcal{E}_{\mathbf{m}}(\mathbf{r}) = i\omega_{\mathbf{m}} \mathcal{A}_{\mathbf{m}}(\mathbf{r})$.

To derive the equation of motion for the electric field defined in Eq. (9) in an open cavity subjected to a coherent pump drive, we use the Lindblad equation,

$$i\hbar \frac{\partial}{\partial t} \hat{\rho} = [\hat{H}_{\text{total}}, \hat{\rho}] + \hat{\mathcal{L}}, \quad (10)$$

where

$$\hat{\mathcal{L}} = \sum_{\mathbf{m}} \left(2\hbar\kappa \hat{a}_{\mathbf{m}} \hat{\rho} \hat{a}_{\mathbf{m}}^{\dagger} - \hbar\kappa \{ \hat{a}_{\mathbf{m}}^{\dagger} \hat{a}_{\mathbf{m}}, \hat{\rho} \} \right) \quad (11)$$

is the Lindbladian term representing cavity losses at constant rate κ . Moreover, $\hat{H}_{\text{total}} = \hat{H}' + \hat{H}_{\text{drive}}$, with \hat{H}' the effective photon-photon Hamiltonian derived in the previous section,

$$\hat{H}' = \sum_{\mathbf{m}} \hbar\omega_{\mathbf{m}} \hat{a}_{\mathbf{m}}^{\dagger} \hat{a}_{\mathbf{m}} + \sum_{\mathbf{m}, \mathbf{n}, \mathbf{p}, \mathbf{q}} \gamma_{\mathbf{m}, \mathbf{n}}^{\mathbf{p}, \mathbf{q}} \hat{a}_{\mathbf{m}}^{\dagger} \hat{a}_{\mathbf{n}}^{\dagger} \hat{a}_{\mathbf{p}} \hat{a}_{\mathbf{q}}, \quad (12)$$

and

$$\hat{H}_{\text{drive}} = i\hbar \sum_{\mathbf{m}} \left(F_{\mathbf{m}} \hat{a}_{\mathbf{m}}^{\dagger} + F_{\mathbf{m}}^* \hat{a}_{\mathbf{m}} \right) \quad (13)$$

the driving Hamiltonian modeling the coherent photon injection in the cavity due to the pump field $\mathbf{E}_{\mathbf{p}}(\mathbf{r})$. The scalar functions $F_{\mathbf{m}}$ are defined as $F_{\mathbf{m}} = \Gamma \int d\mathbf{r} \mathcal{E}_{\mathbf{m}}^*(\mathbf{r}) \cdot \mathbf{E}_{\mathbf{p}}(\mathbf{r})$, where Γ is the pump rate.

From the definition $\phi_{\mathbf{m}} = \text{Tr}(\hat{a}_{\mathbf{m}} \hat{\rho})$ and using Eq. (10), it follows that

$$i\hbar \frac{\partial}{\partial t} \phi_{\mathbf{m}} = \left(\hbar\omega_{\mathbf{m}} - i\hbar\kappa \right) \phi_{\mathbf{m}} + \sum_{\mathbf{n}, \mathbf{p}, \mathbf{q}} \left(\gamma_{\mathbf{m}, \mathbf{n}}^{\mathbf{p}, \mathbf{q}} + \gamma_{\mathbf{n}, \mathbf{m}}^{\mathbf{p}, \mathbf{q}} \right) \langle \hat{a}_{\mathbf{n}}^{\dagger} \hat{a}_{\mathbf{p}} \hat{a}_{\mathbf{q}} \rangle + \hbar F_{\mathbf{m}}. \quad (14)$$

The correlator $\langle \hat{a}_{\mathbf{n}}^{\dagger} \hat{a}_{\mathbf{p}} \hat{a}_{\mathbf{q}} \rangle$ can be added to the system as a dynamical variable after calculating the corresponding equation of motion. However, by noting that $\langle \hat{a}_{\mathbf{n}}^{\dagger} \hat{a}_{\mathbf{p}} \hat{a}_{\mathbf{q}} \rangle$ can be expanded as

$$\begin{aligned} \langle \hat{a}_{\mathbf{n}}^{\dagger} \hat{a}_{\mathbf{p}} \hat{a}_{\mathbf{q}} \rangle &= \phi_{\mathbf{n}}^* \phi_{\mathbf{p}} \phi_{\mathbf{q}} + \phi_{\mathbf{n}}^* \langle \delta\hat{a}_{\mathbf{p}} \delta\hat{a}_{\mathbf{q}} \rangle + \phi_{\mathbf{q}} \langle \delta\hat{a}_{\mathbf{n}}^{\dagger} \delta\hat{a}_{\mathbf{p}} \rangle \\ &+ \phi_{\mathbf{p}} \langle \delta\hat{a}_{\mathbf{n}}^{\dagger} \delta\hat{a}_{\mathbf{q}} \rangle + \langle \delta\hat{a}_{\mathbf{n}}^{\dagger} \delta\hat{a}_{\mathbf{p}} \delta\hat{a}_{\mathbf{q}} \rangle, \end{aligned} \quad (15)$$

we conclude that the quantum-mechanical corrections appear only at second order in the fluctuations. When the field fluctuations are small comparing to the classical value, we may neglect second-order terms and obtain a closed set of equations for the amplitudes,

$$i\hbar \frac{\partial}{\partial t} \phi_{\mathbf{m}} = \left(\hbar\omega_{\mathbf{m}} - i\hbar\kappa \right) \phi_{\mathbf{m}} + \sum_{\mathbf{n}, \mathbf{p}, \mathbf{q}} \left(\gamma_{\mathbf{m}, \mathbf{n}}^{\mathbf{p}, \mathbf{q}} + \gamma_{\mathbf{n}, \mathbf{m}}^{\mathbf{p}, \mathbf{q}} \right) \phi_{\mathbf{n}}^* \phi_{\mathbf{p}} \phi_{\mathbf{q}} + \hbar F_{\mathbf{m}}. \quad (16)$$

Equations (9) and (16) determine the time evolution of the classical field to be

$$i\hbar \frac{\partial}{\partial t} \mathbf{E}^{(+)}(\mathbf{r}) = \sum_{\mathbf{m}} \hbar \left(\omega_{\mathbf{m}} - i\kappa \right) \mathcal{E}_{\mathbf{m}}(\mathbf{r}) \phi_{\mathbf{m}} + \hbar \Gamma \mathbf{E}_{\mathbf{p}}(\mathbf{r}) + \sum_{\mathbf{m}, \mathbf{n}, \mathbf{p}, \mathbf{q}} \mathcal{E}_{\mathbf{m}}(\mathbf{r}) \left(\gamma_{\mathbf{m}, \mathbf{n}}^{\mathbf{p}, \mathbf{q}} + \gamma_{\mathbf{n}, \mathbf{m}}^{\mathbf{p}, \mathbf{q}} \right) \phi_{\mathbf{n}}^* \phi_{\mathbf{p}} \phi_{\mathbf{q}} \quad (17)$$

where the last term on the right-hand side was obtained with the help of the orthogonality condition

$$\int d\mathbf{r} \mathcal{E}_{\mathbf{m}}^*(\mathbf{r}) \cdot \mathcal{E}_{\mathbf{n}}(\mathbf{r}) = \delta_{\mathbf{m}, \mathbf{n}}. \quad (18)$$

Additionally, the first term can be easily simplified by using the definition for mode functions,

$$\hbar\omega_{\mathbf{m}} \mathcal{E}_{\mathbf{m}}(\mathbf{r}) = \left[-\frac{\hbar^2}{2M} \nabla_{\perp}^2 + V_{\text{trap}}(\mathbf{r}_{\perp}) \right] \mathcal{E}_{\mathbf{m}}(\mathbf{r}).$$

Focusing on the two interacting terms, we start by simplifying the first, which we denote by \mathbf{U}_1 . Explicitly, we have

$$\mathbf{U}_1 = -\frac{4e^4}{m^2} \frac{1}{\mathcal{V}^2} \int d\mathbf{r}' \int d\mathbf{r}'' \sum_{\mathbf{k}, \mathbf{k}', \mathbf{m}, \mathbf{n}, \mathbf{p}, \mathbf{q}} f_{\mathbf{k}'} (1 - f_{\mathbf{k}}) \frac{\phi_{\mathbf{n}}^* \phi_{\mathbf{p}} \phi_{\mathbf{q}} e^{i(\mathbf{k}' - \mathbf{k}) \cdot (\mathbf{r}' - \mathbf{r}'')}}{\varepsilon_{\mathbf{k}} - \varepsilon_{\mathbf{k}'} + \hbar(\omega_{\mathbf{m}} - \omega_{\mathbf{q}})} \mathcal{E}_{\mathbf{m}}(\mathbf{r}) \left[\mathcal{A}_{\mathbf{q}}(\mathbf{r}') \cdot \mathcal{A}_{\mathbf{m}}(\mathbf{r}') \right] \left[\mathcal{A}_{\mathbf{p}}(\mathbf{r}'') \cdot \mathcal{A}_{\mathbf{n}}(\mathbf{r}'') \right]. \quad (19)$$

Our goal now is to isolate three electric field terms from the integrand, which requires computing the sums over modes. In full generality this is not possible due to the energy term $\omega_{\mathbf{m}} - \omega_{\mathbf{q}}$ in the denominator, preventing the sums

to be calculated exactly. An approximation is thus required to advance further, which consists in taking into account the typical dimensions of the microcavity, $D_0 \sim 10 - 100 \mu\text{m}$ and $R \sim 0.1 \text{ m}$. This provides a photon-energy spacing of the order $\Delta \sim 100 \text{ GHz}$. Assuming that $\varepsilon_{\mathbf{k}} - \varepsilon_{\mathbf{k}'}$ is of the order of the Fermi energy, we conclude that the term $\hbar\omega_{\mathbf{m}} - \hbar\omega_{\mathbf{q}}$ can be safely neglected from the denominator. Also, we approximate $\mathcal{E}_{\mathbf{m}}(\mathbf{r}) \simeq i\omega_0 \mathcal{A}_{\mathbf{m}}(\mathbf{r})$ and obtain

$$\begin{aligned} \mathbf{U}_1 &= \frac{4e^4}{m^2\omega_0^3} \frac{i}{\mathcal{V}^2} \sum_{\mathbf{k}\mathbf{k}'} f_{\mathbf{k}'}(1-f_{\mathbf{k}}) \int d\mathbf{r}' \int d\mathbf{r}'' \frac{e^{i(\mathbf{k}'-\mathbf{k})\cdot(\mathbf{r}'-\mathbf{r}'')}}{\varepsilon_{\mathbf{k}}-\varepsilon_{\mathbf{k}'}} \sum_{\mathbf{m}\mathbf{n}\mathbf{p}\mathbf{q}} \mathcal{E}_{\mathbf{m}}(\mathbf{r}) [\mathcal{E}_{\mathbf{q}}(\mathbf{r}') \cdot \mathcal{A}_{\mathbf{m}}(\mathbf{r}')] [\mathcal{E}_{\mathbf{p}}(\mathbf{r}'') \cdot \mathcal{E}_{\mathbf{n}}(\mathbf{r}'')] \phi_{\mathbf{n}}^* \phi_{\mathbf{p}} \phi_{\mathbf{q}}, \\ &= \frac{4e^4}{m^2\omega_0^3} \frac{i}{\mathcal{V}^2} \sum_{\mathbf{k}\mathbf{k}'} f_{\mathbf{k}'}(1-f_{\mathbf{k}}) \int d\mathbf{r}' \int d\mathbf{r}'' \frac{e^{i(\mathbf{k}'-\mathbf{k})\cdot(\mathbf{r}'-\mathbf{r}'')}}{\varepsilon_{\mathbf{k}}-\varepsilon_{\mathbf{k}'}} \sum_{\mathbf{m}} \mathcal{E}_{\mathbf{m}}(\mathbf{r}) [\mathcal{A}_{\mathbf{m}}(\mathbf{r}') \cdot \mathbf{E}^{(+)}(\mathbf{r}')] |\mathbf{E}(\mathbf{r}'')|^2. \end{aligned} \quad (20)$$

Using the orthogonality of the photon-mode functions,

$$\sum_{\mathbf{m}} \mathcal{E}_{\mathbf{m}}(\mathbf{r}) \cdot \mathcal{A}_{\mathbf{m}}(\mathbf{r}') = \frac{i\hbar}{2\varepsilon_0} \delta(\mathbf{r}-\mathbf{r}'), \quad (21)$$

in Eq. (20), we are led to the final expression:

$$\begin{aligned} \mathbf{U}_1 &= -\frac{2e^4\hbar}{m^2\varepsilon_0\omega_0^3} \frac{1}{\mathcal{V}^2} \sum_{\mathbf{k}\mathbf{k}'} f_{\mathbf{k}'}(1-f_{\mathbf{k}}) \frac{1}{\varepsilon_{\mathbf{k}}-\varepsilon_{\mathbf{k}'}} \int d\mathbf{r}'' e^{i(\mathbf{k}'-\mathbf{k})\cdot(\mathbf{r}-\mathbf{r}'')} |\mathbf{E}(\mathbf{r}'')|^2 \mathbf{E}^{(+)}(\mathbf{r}), \\ &= -\frac{2e^4\hbar}{m^2\varepsilon_0\omega_0^3} \frac{1}{\mathcal{V}^2} \sum_{\mathbf{k}\mathbf{k}'} f_{\mathbf{k}'}(1-f_{\mathbf{k}'-\mathbf{k}}) \frac{1}{\varepsilon_{\mathbf{k}'-\mathbf{k}}-\varepsilon_{\mathbf{k}'}} \int d\mathbf{r}'' e^{i\mathbf{k}\cdot(\mathbf{r}-\mathbf{r}'')} |\mathbf{E}(\mathbf{r}'')|^2 \mathbf{E}^{(+)}(\mathbf{r}). \end{aligned}$$

A similar route can be followed to find that $\mathbf{U}_2 = \mathbf{U}_1$, and we arrive at

$$\begin{aligned} i\hbar \frac{\partial}{\partial t} \mathbf{E}^{(+)}(\mathbf{r}, t) &= \left[-\frac{\hbar^2}{2M} \nabla_{\perp}^2 + V_{\text{trap}}(\mathbf{r}_{\perp}) - i\hbar\kappa \right] \mathbf{E}^{(+)}(\mathbf{r}, t) \\ &+ \hbar\Gamma \mathbf{E}_{\mathbf{p}}(\mathbf{r}) + \int d\mathbf{r}' g(\mathbf{r}-\mathbf{r}') |\mathbf{E}(\mathbf{r}', t)|^2 \mathbf{E}^{(+)}(\mathbf{r}, t), \end{aligned} \quad (22)$$

where

$$g(\mathbf{r}) = -\frac{4e^4\hbar}{m^2\varepsilon_0\omega_0^3} \frac{1}{\mathcal{V}^2} \sum_{\mathbf{k}, \mathbf{k}'} e^{i\mathbf{k}\cdot\mathbf{r}} \frac{f_{\mathbf{k}'}(1-f_{\mathbf{k}'-\mathbf{k}})}{\varepsilon_{\mathbf{k}'-\mathbf{k}}-\varepsilon_{\mathbf{k}'}} \quad (23)$$

is the effective photon-photon coupling controlled by the state of the plasma through its distribution function.

The GP equation derived here is an effective equation of motion for nonlinear quantum optics in a driven-dissipative cavity. It is important to emphasize that it is *not* an equilibrium order-parameter equation implying photon Bose-Einstein condensation. No number conservation or thermalization is assumed. Equation (22) follows from interacting light-matter effects in a medium with a nonlocal, plasma-mediated susceptibility, and its GP-like structure simply reflects the classical-field limit of the coherent cavity mode. This places our analysis squarely within nonlinear quantum optics (driven-dissipative quantum theory), rather than equilibrium Bose condensation.

III. EXPERIMENTAL SET-UP DESIGN

Figure 1 summarizes the architecture we propose to realize the mixed coupling required for supersolidity. The

cavity supports a standing wave along the growth axis z , and the two GaAs QWs are positioned at consecutive antinodes of $|E(z)|^2$. This placement maximizes the photonic sampling of each electron sheet and renders the coupling robust to small thickness errors, since $\partial_z |E|^2 = 0$ at the maxima. With the QWs at antinodes, the effective interaction kernel is the weighted sum

$$g(k) = w_1 g_{\text{deg}}(k) + w_2 g_{\text{th}}(k), \quad (24)$$

where w_j are set by the local field intensity at each QW and by their axial positions in the standing wave.

The heterostructure inside the spacer is engineered to host two electronically independent 2DEGs. Starting from the top mirror and moving downward, an $\text{Al}_{0.3}\text{Ga}_{0.7}\text{As}$ barrier of 8–12 nm separates a Si δ -doping plane (effective thickness $< 1 \text{ nm}$; sheet $N_D \simeq (1.0-1.6) \times 10^{12} \text{ cm}^{-2}$) from QW1 (GaAs, 7–10 nm). A subsequent $\text{Al}_{0.3}\text{Ga}_{0.7}\text{As}$ barrier of 5–10 nm completes the confinement. The two wells are then isolated by a high-Al barrier $\text{Al}_{0.9}\text{Ga}_{0.1}\text{As}$ of 30–50 nm, which suppresses tunneling and minimizes interlayer Coulomb drag in the absence of in-plane currents. Below the separator, a second $\text{Al}_{0.3}\text{Ga}_{0.7}\text{As}$ setback layer of 15–25 nm precedes the lower Si δ -plane ($< 1 \text{ nm}$; $N_D \simeq (1-3) \times 10^{11} \text{ cm}^{-2}$) and QW2 (GaAs, 7–10 nm), followed by another 5–10 nm $\text{Al}_{0.3}\text{Ga}_{0.7}\text{As}$ barrier and the bottom GaAs/AlAs DBR. The δ -planes are fixed donor sheets embedded in AlGaAs, which ionize and electrons transfer into the lower-energy GaAs wells due to the band offset and confinement. The *setback* d (distance between the δ -plane and the QW) controls the baseline sheet density n_j of each QW and the level of remote-impurity scattering. Smaller d in-

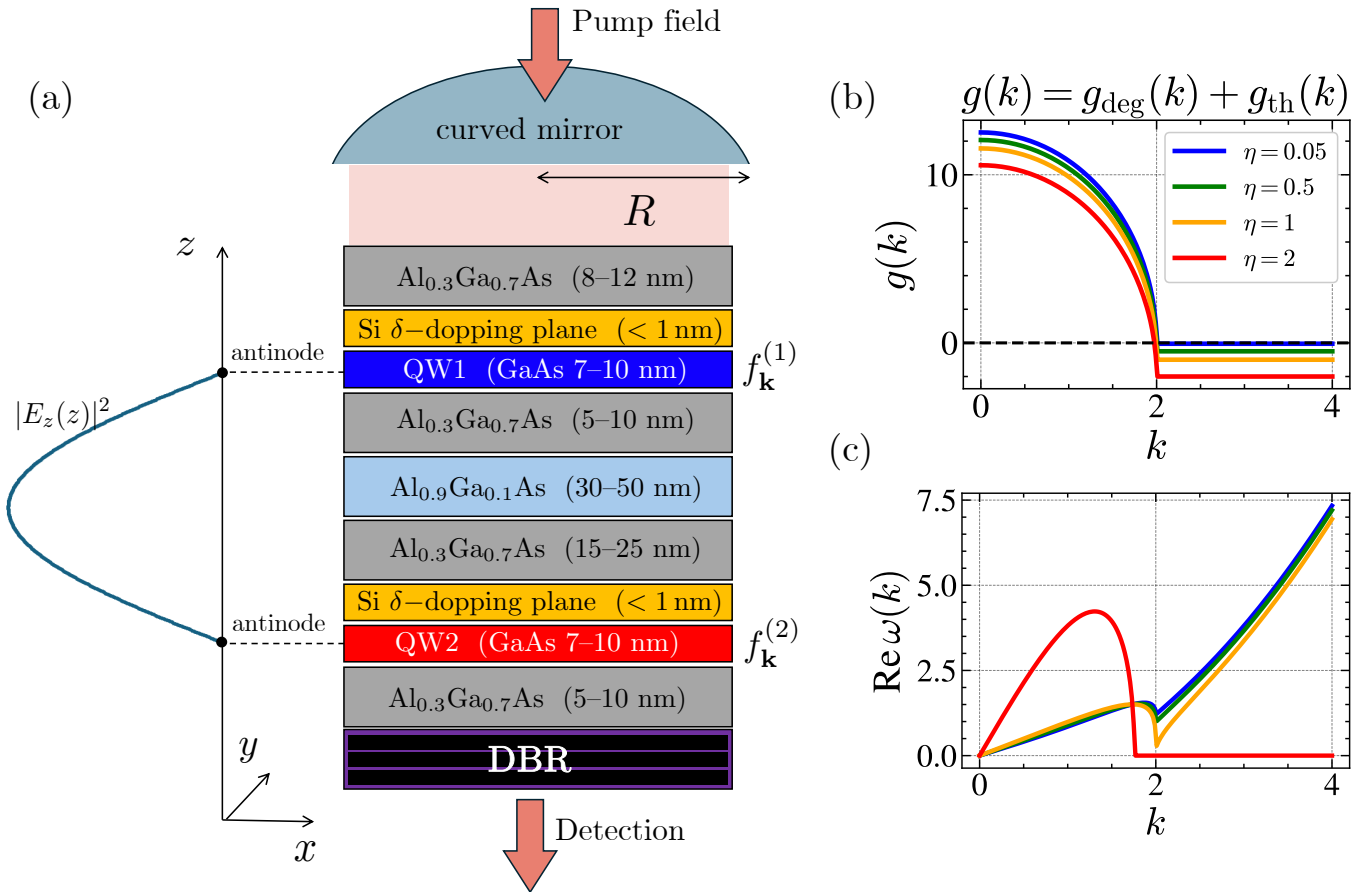


FIG. 1: (a) Experimental set-up to detect the supersolid phase. A curved top mirror and a GaAs/AlAs bottom DBR form a cavity that hosts two GaAs quantum wells (QWs) placed at consecutive antinodes of the longitudinal intracavity intensity profile $|E_z(z)|^2$ (sketch at left; dashed lines mark the antinodes). QW1 is tuned degenerate and QW2 nondegenerate by remote δ -doping with different setbacks; a wide-gap $\text{Al}_{0.9}\text{Ga}_{0.1}\text{As}$ barrier suppresses tunneling and interlayer drag. A coherent pump field enters from the top, and detection is made through the bottom DBR. Layers are not to scale. (b) Plot of the effective kernel of Eq. (24) for several values of local coupling η with fixed $\alpha = 0.4$, $\Gamma = 1$ and $\kappa = 0.1$ and (c) corresponding real part of the frequency.

creases n_j but raises Drude loss, and larger d reduces n_j and scattering but can underfill the well if it becomes too large. Choosing $d = 8\text{--}12$ nm with the higher N_D above QW1 and $d = 15\text{--}25$ nm with the lighter N_D above QW2 yields the contrasting electronic regimes required below.

Electrically, each QW resides in an isolated mesa with independent ohmic contacts and a transparent top gate [ITO (10–15 nm) on Al_2O_3 (10–20 nm)], enabling in situ trimming of n_j without cross talk. Under room-temperature conditions we target, for QW1 (degenerate), a sheet density $n_1 \simeq \times 10^{12} \text{ cm}^{-2}$, corresponding to $T_F \simeq 450$ K ($m = 0.067m_e$ for GaAs); and for QW2

(nondegenerate), $n_2 \simeq (1\text{--}3) \times 10^{10} \text{ cm}^{-2}$, corresponding to $T_F \simeq 4\text{--}12$ K. The large-Al separator together with sub-gap operation ensures that the electronic distributions $f_{\mathbf{k}}^{(1)}$ and $f_{\mathbf{k}}^{(2)}$ remain stationary and effectively independent on photonic time scales.

The cavity is driven from the top at 950 nm, near the $k \simeq 0$ resonance and below the GaAs gap, with typical detunings $\Delta = \pm(1\text{--}3)$ meV, 20–30 μm FWHM spot, and on-sample power 0.1–1 mW for $Q \simeq 10^5$. Sub-gap pumping avoids interband excitation so that hole contributions are negligible, and the bottom DBR is used for detection.

[1] Kuramoto, Y. (2020). Quantum Many-Body Physics: A Perspective on Strong Correlations (1st ed., Lecture Notes

in Physics, Vol. 934). Springer Tokyo.